PCCP

On the STM imaging contrast of graphite: towards a "true" atomic resolution

F. Atamny,* O. Spillecke and R. Schlögl

Fritz-Haber-Institut der Max-Planck-Gesellschaft, Faradayweg 4-6, 14195 Berlin (Dahlem), Germany

Received 11th June 1999, Accepted 8th July 1999

Different phenomena observed in the high-resolution images of graphite by scanning tunneling microscopy (STM) or atomic force microscopy (AFM) such as the asymmetry in the charge density of neighboring carbon atoms in a hexagon, the high corrugation amplitudes and the apparent absence of point defects has led to a controversial discussion since the first published STM images of graphite. Different theoretical concepts and hypotheses have been developed to explain these phenomena. Despite these efforts a generally accepted interpretation is still lacking. In this paper we discuss a possible imaging mechanism based on mechanical considerations. Forces acting between tip and sample are taken into account to explain the image contrast. We present for the first time a direct atomic resolution of the graphite hexagonal structure by transmission electron microscopy (HRTEM), revealing the expected hexagonal array of atoms and the existence of several types of defects. We discuss the possibility that the STM image of graphite is a result of convolution of the electronic properties and the atomic hardness of graphite.

Introduction

Atomic resolution of graphite by scanning probe techniques has become a routine procedure. Many features, phenomena and anomalous STM images have thus been collected and attempts made to interpret them.[1–3] Considerable effort has been expended to understand the imaging mechanism behind these phenomena since the invention of the STM in 1982.[4] Despite extensive studies, several important issues concerning the STM imaging of graphite, such as the atomic resolution of graphite and imaging of atomic-scale defects (*e.g.* point defects, steps *etc.*) are not yet well understood.

The fact that in most STM images of graphite one observes with positive contrast only three of the six carbon atoms[2,5,6] from the hexagon of the graphite lattice (see Fig. 3 below) has caused controversial discussions. Several theoretical concepts and hypotheses have been suggested to explain this apparent asymmetry in the charge density of neighboring carbon atoms. The concepts can be divided in three mean categories: (a) theories attributing this asymmetry to purely electronic effects, (b) a theory which ascribes the asymmetry and other phenomena such as Moiré patterns to both electronic and mechanical origins and (c) a hypothesis which describes the asymmetry as a result of only mechanical effects. A fourth category which considers interference phenomena occurring between two or more images detected by multiple mini tips,[7] or between special tip electronic levels and sample surface[8] or between top layer and sublayer,[9] has been proposed to rationalize several types of anomalous STM images, such as triangular arrays of triangles, honeycomb arrays and triangular arrays of ellipses or linear row-like structures[7] and Moiré patterns.

The theoretical concepts which consider only electronic effects in explaining the STM contrast of graphite are represented by Tomanek *et al.*,[10,11] Tersoff,[12] and Tchougreeff and Hoffmann.[13] They assume different electronic effects and treat them from different theoretical viewpoints.

Tomanek *et al.*[10,11] attribute the asymmetry[14] to interlayer interactions between the top layer and the layer located directly below and to the structural site asymmetry of the hexagonal graphite. These interactions and the site asymmetry render the carbon atoms of the surface layer non-equivalent. Fig. 1 illustrates the assumed non-equivalent types of carbon atoms. The A-type carbon atoms (Fig. 1(a)) in hexagonal graphite (with ABAB stacking) have neighbors directly below in the second layer, whereas the B-type atoms are located above the centers of the hexagons of the layer beneath. Thus, differences in the LDOS (local density of states) occur as a consequence of the resulting interlayer interactions. Because these states are relevant[15] for the detected tunneling current such asymmetry is observed by STM. Tomanek *et al.*[10,11] show in their model: (a) that the atoms visible in the STM image are of the B-type, (b) the asymmetry should be nearly independent of the polarity of the bias voltage, and (c) an increase of the bias voltage should decrease the asymmetry.

Based on the suggestions of Tomanek *et al.* several theoretical calculations have been performed using different concepts such as the extended Hückel tight binding method[16] and *ab initio* periodic Hartee–Fock calculations.[17] All studies yielded similar results, supporting the predictions of Tomanek *et al.*

Tersoff,[12] using a graphene layer (*i.e.* a monolayer of graphite) and plane wave functions, ascribes the large corrugations to the unusual electronic structure of a single graphene layer in which the Fermi surface collapses to a point at the corner of the surface Brillouin zone. Thus, the STM image corresponds to an individual state. The nodal structure of this state gives rise to a large corrugation with the periodicity of the unit cell, independent of the atomic positions within the unit cell. Although this interesting theoretical treatment has found favour with many researchers, others have doubted its correctness.[17]

Despite the general acceptance of the theoretical concept of Tomanek *et al.*,[10,11] this model is, however, not consistent with the experimental observations made on only one graphene layer on Pt(111)[18] and with data from graphite intercalation compounds[19–21] where, also, only three of the six carbon atoms of the hexagon lattice have been imaged although, in both cases, the structural asymmetry between the A and B sites is removed. Tchougreeff and Hoffmann[13]

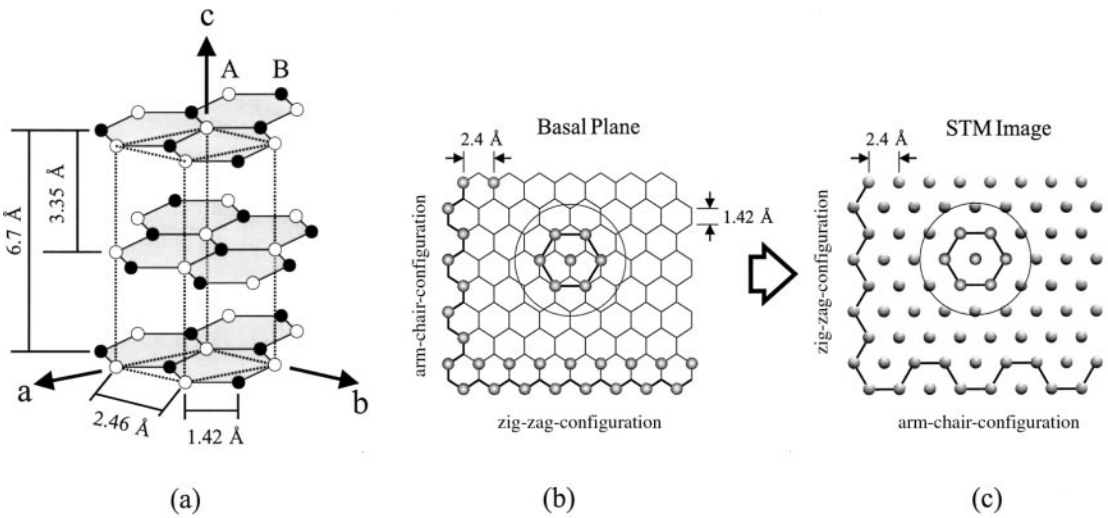

Fig. 1 (a) Schematic representation of the structure of the bulk hexagonal graphite crystal (ABAB stacking), showing the two non-equivalent types of carbon atom sites: A-types (○) have neighbors directly below in the second layer, and B-types are located above an hexagon (●). The dashed lines show the bulk unit cell. The in-layer nearest carbon–carbon distance is 1.42 Å and carbon layers are separated by 3.35 Å. (b) Top view of the basal plane of graphite. (c) Schematic representation of the surface structure (carbon atoms) of graphite most viewed by STM, where every other atom is enhanced. "Zig-zag-" and "arm-chair-configuration" of the edges of a graphite (0001) face are also seen. Note the change of the positions of the two configurations.

explained these results by extending the concept proposed by Tersoff,[12] in which the intrinsic electron structure of a graphene layer is considered. They attributed the non-equivalency of the A and B sites to electron–electron interactions within a single layer and constructed a model describing the total energy in a graphene layer by including four terms, describing (a) the electron transfer from A and B sites in the (*m*,*l*)-th unit cell to adjacent sites both inside and outside the unit cell, (b) the repulsion between electrons when they happen to occupy the same sites, (c) the repulsion between electrons occupying adjacent sites, and (d) the attraction of electrons to the cores of the adjacent carbon atoms. To find the ground state of a graphene layer they constructed an electron–electron-interaction phase diagram for graphite in a space defined by the magnitude of on-site and nearest-neighbor electron repulsion. In the phase diagram the spin density wave (SDW), the charge density wave (CDW), and the metallic (M) ground states are included, representing the metallic and both insulating (with spin or with charge order) regions. In a chemical picture, this hypothesis quantized the "aromaticity" of graphite and introduced fractional double-bond localization. Thus, a description of the graphene layer in different areas of the electronic parameter space was obtained, allowing a consideration of what effect these features of the electronic structure might have on the observed STM image of graphite.

Based on the suggestion of Tersoff,[15] where the observed STM image is the constant conductance surface, they showed that for the metallic phase the LDOS at the A and B sites (in a graphene layer) are equal, and the conductance does not depend on whether the tip is positioned above the A or the B site. In the case of the CDW ground state the opposite happens. The upper and lower bands are separated by a gap, where only the lower band gives a contribution to the LDOS at the Fermi level. For that reason the LDOS at the A and B sites are not equal, leading to a conductance dependence on the position of the tip. In the SDW state of the graphene layer, which has the lowest energy in the phase diagram, the total electron density and the LDOS do not depend on the site. The spin density, however, depends on it, and spin-up electrons are concentrated on the A sites, whereas spin-down electrons are located preferably on the B sites. Based on this treatment of the electronic structure of the graphene layer, Tchougreeff and Hoffmann concluded that low-symmetry states of both types (SDW and CDW) may be responsible for the observed STM images of the surface of bulk graphite and of the graphene layer as well.

In this study, however, the independence of the asymmetry on the polarity of the bias voltage is not examined. Whangbo *et al.*[16] extended the considerations of Tchougreeff and Hoffmann[13] and showed that a dependence of the asymmetry on the polarity is expected, which is not in agreement with experimental findings. Thus, they summarize that the asymmetry is not caused by a CDW or SDW state of graphene layer.

Whangbo *et al.*[16] discussed an approach in which both electronic and mechanical effects were considered. Using extended Hückel tight-binding calculations they show that the local hardness has to be taken into account to achieve an appropriate explanation for the appearance of the asymmetry observed in simultaneously imaged STM/atomic force microscopy (AFM) pictures on graphite and for the appearance of superstructures (superperiodicity) of hexagonal symmetry.[9,22] They emphasize that for the interpretation of the STM and AFM images of layered materials such as graphite, an analysis based on the partial density plot ($\rho(r_0, E_f)$; where r_0 is the tip–surface distance and E_f is the Fermi-level) and total density plot ($\rho(r_0)$) is insufficient, and that it is necessary to take into account the local hardness of the surface layer. The comparison of simultaneously observed STM/AFM images leads to the conclusion that the positions of the atoms seen in AFM images correspond to the positions of the atoms of the B-type in STM images. Based on the consideration that the tip exerts a mechanical force on the surface[5,23–25] and, consequently, morphological changes of the graphite surface occur, they show that these morphological changes vary with the local hardness variation. Consequently, they conclude that the B-site is depressed less than the A-site by the tip force, *i.e.* the B-site is harder than the A-site.

Other theoretical concepts have also been suggested that consider mechanical effects in explaining the asymmetry in the charge density and the increased corrugation amplitudes in STM images of graphite. Soler *et al.*[23] explain the corrugation amplitudes by elastic deformation of the upper graphite layers induced by interatomic forces between tip and surface. They emphasize that this explanation seems to be especially plausible because graphite is a soft material. Based on the study of Soler *et al.*,[23] Pethica[26] and Batra *et al.*[27] discussed the possibility that imaging a simple periodic structure could also be achieved by the sliding of graphite planes just beneath the tip caused by the lateral tip movement. The charge density

increases at the minima in the graphite rings as the layer stacking shears out of its equilibrium (symmetry) position. Shear over a complete lattice period therefore produces a single-cycle increase and decrease of the tunneling current. Thus, a fluctuation in tunneling current occurs, as required, reflecting the lattice periodicity as the tip is scanned over the surface. An indication of the feasibility of such an imaging mechanism is the experimental results of Smith *et al.*[28] They were even able to image atomic periodicity on graphite by collapsing the potential barrier between tip and sample (macroscopic tip–sample contact).

In this paper we discuss a possible imaging mechanism of graphite based on mechanical considerations, in which tip–surface interactions, local surface elastic deformation, and local hardness are addressed. We support this hypothesis by comparing STM/AFM measurements with high-resolution transmission electron microscopy (HRTEM) results that have been recently achieved for the first time.

Results and discussion

Fig. 2 shows a high-resolution transmission electron micrograph (HRTEM) of graphite. Such a lattice resolution of the basal plane ((001)face) has been achieved for the first time using HRTEM. Bright hexagonal rings with a side length of (*d*) 1.42 Å are seen, corresponding to the atomic distance between two adjacent carbon atoms in graphite. The centers of the rings appear as dark holes. The distance between the centers of the holes is 2.46 Å. The close-packed array of hexagonal rings reflects the well-known graphite structure. The variation in the contrast over large areas seen in the micrograph is attributed to turbostatic disorder[29] of the stacked graphite layers. The continuous variation in contrast shows that an ABAB stacking with well-aligned columns of atoms along [001] only exists as an average over large areas, as seen in Fig. 2 and over a sample thickness of about 20 nm. The two-dimensional projection of several graphene sheets along [100] renders it difficult to identify point defects, as local contrast variations around single hexagons (see *e.g.* center of inset or center of large image) may well arise from stacking disorder.

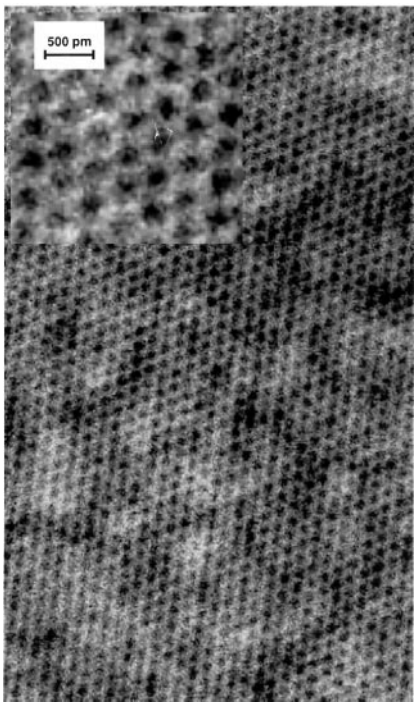

Fig. 2 HRTEM micrograph of a HOPG sample, revealing hexagonal rings with side lengths of 1.42 Å. The centers of the rings appear as dark spots. The inset shows a higher magnification.

Fig. 3 shows an STM image and its inverted contrast observed on graphite. The gray-scale image depicts bright spots (with a distance of 2.46 Å between the top of spots), holes and saddle spots with less intensity in-between. This is further illustrated by the corresponding cross section scans. Two peaks are seen in the cross section of the STM image. According to the imaging mechanism theory of Tomanek *et al.*,[10,11] the bright spots with the higher intensity (*i.e.* corrugation: 0.8 Å) correspond to the B-site atoms and the spots with less intensity (*i.e.* corrugation: 0.2 Å) to the A-site. Since the STM measurements have been performed with a bias voltage of 200 mV a variation in the peak registry, is expected.[10,11] However, the changes in the relative corrugations in the image (*i.e* the asymmetry between A- and B-sites and the height relations between A-, B- and hollow-sites)[10,11] differs from the calculated model results.[2,10] Tomanek *et al.*[10] predict an asymmetry of less than 0.3 Å at a bias voltage of 200 mV. In our case the asymmetry is 0.6 and the height relation is 0 : 1 : 4 (hollow : A-site : B-site). In other words, the A-sites are less and the B-sites are more pronounced in the experiment than in the model. These observations are not new.[2] They have been confirmed several times in the past in previous studies performed under various conditions by different research groups.[6] The origin of this discrepancy between reproducible experiments and the model has been controversially discussed. While Tersoff[12] attributes it to pure electronic effects, Mamin *et al.*[5] and Mate *et al.*[24] ascribe it to mechanical deformation of the sample surface induced by the force interaction between tip and sample. The latter explanation seems, however, to be particularly suitable for understanding the appearance of giant corrugations of 8 Å or even more observed on graphite.[6] The inverted image (Fig. 3(b)) however, reveals changes in the relative corrugations which are consistent with the model calculations. The height relations (see cross section) give a value of 0 : 3 : 4 and an asymmetry of 0.15 that are closer to the calculated values.[2,10]

This observation and other effects described in the introduction, which can not be explained by Tomanek's theory, lead to the assumption that, probably, additional imaging mechanisms are involved in the contrast formation of graphite. These mechanisms are not based only on electronic properties and consist of tip–surface interactions[5,23–25] and the elasticity of graphite layers. Consideration of the idea of Whangbo *et al.*,[16] that the B-site carbon atoms are harder

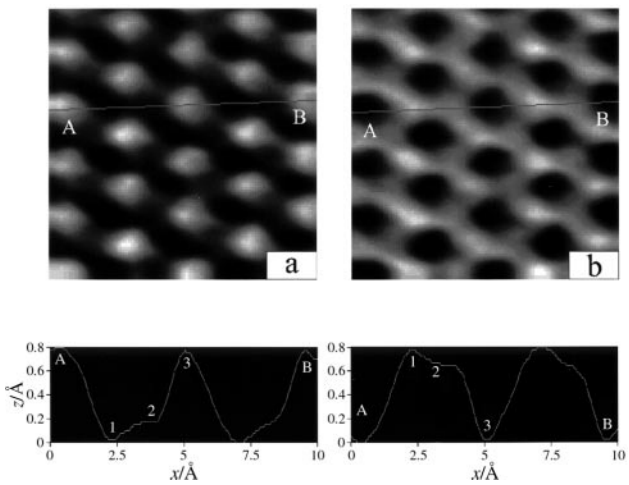

Fig. 3 (a) Typical STM image of graphite, representing the charge density asymmetry of the A- and B-type carbon atoms in graphite. The distance between the bright spots (atoms) is 2.4 Å. The corresponding cross section exhibits the height relations between the surface sites A, B, and hollow. (b) Inverted image showing the inverted contrast of image (a).

than the A-site atoms, and expanding the idea by assuming that a monatomic probe tip depresses not only the one carbon atom located directly under it, but also the other three first-nearest-neighbor carbon atoms linked to the compressed carbon atom, one realizes that the hollow (*i.e.* the carbon-ring center) of a hexagon should be much harder than both other sites (*i.e.* A- and B-site). This is due to the fact that the tip depresses to a first approximation, when it is located above a hollow of not four carbon atoms, as the case when it is positioned over an A- or B-site, but rather six carbon atoms (Fig. 4). This is understandable when we compare the radii of the metal atoms Pt, Ir, and W (1.39, 1.36, and 1.39 Å, respectively)[30] with the radius of a hexagonal ring (1.42 Å). Hence, the most protruded tip atom "sees" due to its size which is comparable to the size of a hexagon, all of the six carbon atoms of a hexagon. Thus, the energy needed to depress a hollow-site is much higher than that needed for depressing an A- or a B-site.[16] It is thus important to note that in the top graphene layer three sites for imaging exist rather than only the two atomic sites A and B considered up to now. Previous studies showed that as the tip initially approaches the surface, the tip experiences repulsive forces before detecting a tunneling current.[24,25] The repulsive force which the tip experiences is in the range 10^{-6}–10^{-7} N. This is at least one order of magnitude more than the repulsive force typically employed in contact-mode AFM measurements.[31,32] Now, taking into account the mechanical force the tip exerts to the surface,[5,23–25] and consequently the tip-induced geometrical distortion of the surface, the STM image can be described as a map of this surface distortion. The STM image is thus a convolution of the surface distortion and the LDOS, since the distortions cause a *z*-displacement of the piezo to maintain a constant value of the tunneling current. In the case of performing measurements in the constant height mode operation, the surface is depressed differently and thus the tip–surface distance varies, resulting in the detection of different tunneling currents. Mate *et al.*[24] show that the force needed to maintain a constant current varies considerably as the tip scans from one part of the graphite unit cell to another. This supports the consideration that variations do exist in the local hardness between A-, B-, and hollow-sites. Since the hollow-site is the hardest one, it is assumed that the STM image

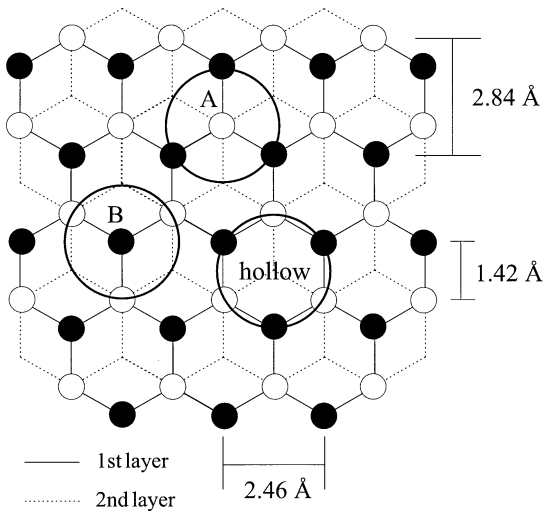

Fig. 4 Schematic representation illustrating the number of carbon atoms in the graphite structure which can be depressed by a tip consisting of an atom on its top part (●) at different positions. When the tip is located above A- or B-sites, three additional carbon atoms can be depressed by, for instance, a metal tip atom (*e.g.* W, Pt, or Ir). Above a hollow-site all of the six carbon atoms of a hexagon are "seen" by the tip, due to its comparable size (*e.g.* Pt, W: 1.39 Å) with the radius of the hexagon (1.42 Å). The size of the solid circle (2.79 Å diameter, corresponds to the diameter of a Pt atom) has been drawn to the same scale as for the hexagons.

reveals an inverse contrast of atom positions in the hexagonal graphite unit cell as illustrated in Fig. 3. The hollow-site appears in the original image as a protrusion, the B-site as a saddle point, and the A-site as a depression. The inverted STM image agrees well with the expected structure. A hexagonal ring is seen with two different types of carbon atoms. This re-interpretation of the contrast in graphite would also explain the many anomalous images obtained by AFM and the atomically resolved AFM images of graphite. In these images, only every other carbon atom is visible, although, according to theoretical calculations of Abraham and Batra,[33] a monatomic tip is expected to image every carbon atom on the graphite surface, leading to a honeycomb lattice. Similar AFM results have also been reported for atomic resolution experiments with boron nitride, another hexagonal layered material.[34] Here only one spot with a periodicity of 2.5 Å (*i.e.*, topographic maximum: "atom") is revealed per unit cell which corresponds to the distance between the centers of two unit cells. This observation may be explained by the above discussed imaging mechanism. The STM thus "sees" not the atoms but the hollow sites which are related to one atom site only by translation symmetry operations.

The existence of a strong mechanical tip–sample interaction can be deduced from additional experiments data, namely from the so-called etching process. Previous STM and AFM studies of various layered materials show that surface etching commonly occurs spontaneously during scanning,[33–38] indicating a relatively strong tip–sample interaction. Weakly bonded material pieces located on the surface as well as destroyed graphene layers[35] are moved from the scanning area by successive STM and AFM scans. Graphene sheets can be folded and even rolled up by using the tip of an AFM[39,40] or a STM.[41–43] Surface etching is more efficient at a smaller tunneling gap resistance R_{gap} ($R_{gap} = V_{bias}/I_t$, where V_{bias} is the bias voltage and I_t is the set-point tunneling current),[38] which is a qualitative measure of the tip–surface distance r_0 since R_{gap} decreases with decreasing r_0, indicating an increase of the contribution of a force-induced modification. Although the origin of etching is not yet clear, it is probable that the etching process involves mechanical tip–surface interactions. This suggestion is supported by the recently performed experiments to manipulate intentionally graphite sheets by modulating the tip–sample distance,[41–43] which is related to modulating the tip–sample interaction. Fig. 5 depicts an example of spontaneous etching which had occurred during scanning. This image of the destroyed upper graphene layer(s) at the chemically produced nanochannel (Fig. 5(a)) can only be understood on the basis of a considerable force interaction between tip and sample.

Rarely, positive contrast STM images of graphite revealed all of the six carbon atoms in a hexagon with the same height corrugation (intensity).[44] Although the origin of such a pheno-

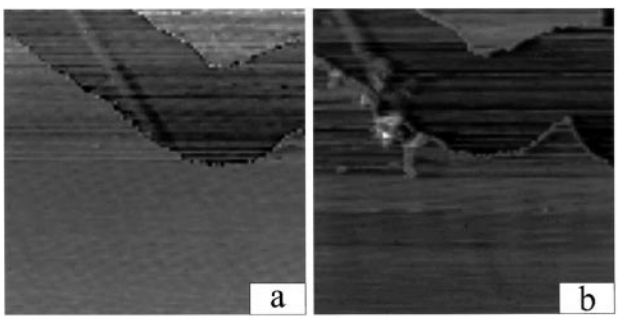

Fig. 5 Two subsequently taken STM images (400 × 400 nm) showing tip-induced etching at a step edge of graphite. (a) A one monolayer deep channel-like feature arise from sample oxidation at elevated temperature (650 °C) is seen. (b) Illustrates the etching process that occurred during scanning over the sample. Parts of the upper graphene sheet have been folded or destroyed.

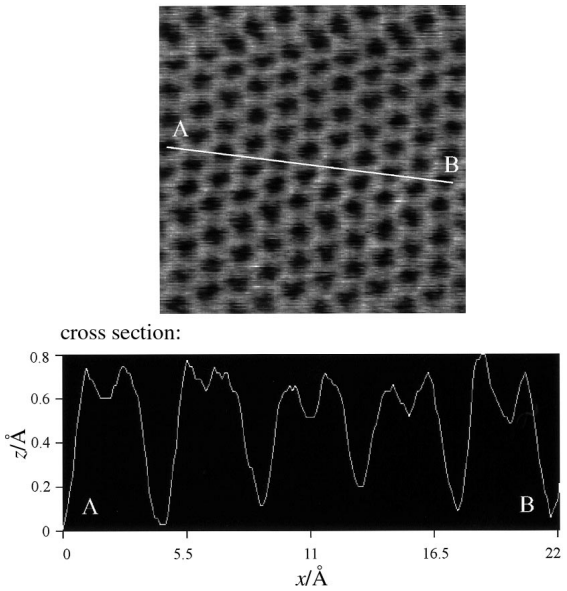

Fig. 6 Atomic resolution STM image of graphite where all of the six carbon atoms of the hexagons are visible. The cross section scan reveals two pronounced maxima corresponding to two adjacent carbon atoms ($d = 1.42$ Å) in a hexagon and valleys in-between showing the variations in the charge density between two adjacent carbon atoms. The distance between the deepest points is 2.46 Å which corresponds to the holes of the hexagonal.

mena is not yet clear, it is probable that the contribution of the mechanical tip–sample interaction is much smaller than that of the tunneling current to the measured corrugation. This may be attributed to a coincidence of several convenient circumstances, such as a graphite flake sticking on the top of the STM tip, which interacts mechanically very weakly with the graphite surface, leading to a negligible contribution of the mechanical tip–sample interaction to the measured STM corrugation. Alternatively, the distance between the tip and the sample coincides with the required conditions where the mechanical tip–sample contribution is minimal.[44] Thus, the mapped corrugation can be described as a purely electronic mapping of the LDOS.

Fig. 6 depicts raw data of a true atomically observed STM image. From the features, one can discern hexagonal rings consisting of equivalent carbon atoms with a hole in the center. This is consistent with the general, valid concept of the graphite structure that all of the six carbon atoms are electronically equivalent, as has very often been confirmed by previous spectroscopic studies probing the local electronic structure of sp^2 carbon atoms.[29] The cross section scan shows two clearly pronounced maxima with almost the same height corrugation (*i.e.* equivalence of the LDOS at the A and B sites) and a valley in-between (*i.e.* along the C–C bond)

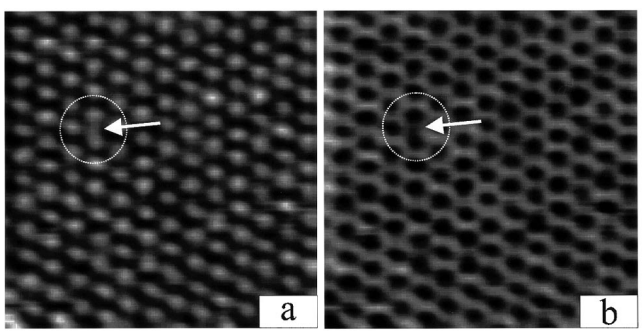

Fig. 7 (a) A gray-scale STM image showing the typical non-equivalence of the graphite sites. In addition to the periodic structure of the spots a bright protrusion between two bright spots (atoms) is seen (arrow). In the inverted image (b) this protrusion appears as a vacancy-like feature (arrow).

showing the variations of the charge density between two adjacent carbon atoms in a hexagon. The shape and size of the hexagonal rings are strikingly similar to these observed with HRTEM (Fig. 2). This leads to the justified assumption that this atomically resolved STM image reveals the true hexagonal configuration of the graphite structure and the fact that such images are not frequently observed is a question of the experimental conditions (*i.e.* minimization or elimination of the contribution of the mechanical tip–sample interaction) under which the images were obtained. In this particular case the amount of tunneling current in relation to the measured corrugation seems to be predominant, leading to an exclusive mapping of the LDOS.

Despite the fact that graphite has been extensively studied and many STM and AFM images have been published, only a few STM/AFM images of point defects[45] of untreated graphite samples have been shown, although the natural defect density in a graphite (HOPG) surface varies between 0.1 and 20 point defects per μm^2 refs. 46 and 47, depending on the quality and history of the HOPG sample. Point defects can be viewed indirectly by creation of etch pits through oxidation reactions. It is known that on the basal plane ((0001) face) only defects (vacancies, steps *etc.*) are attacked by molecular oxygen at elevated temperatures ($>650°$),[48–51] leading to creation of etch pits and recession of steps. Thus, the failure to image point defects frequently is not a question of their existence but rather a problem of the imaging mechanism. This has led to several speculations concerning this topic, including the study of the effect of local defects in a graphite layer on its electronic structure and their manifestation in the STM image.[52–57] There was even doubt over the calibration of the lateral atomic resolution on graphite, since imaging of atomic-scale defects is an important indication of the achievement of a true atomic resolution.[58]

Based on the discussed imaging contrast mechanism of graphite, point defects appear, probably, as protrusions, due to the additional tip interaction with the functional groups bonded to the "free" carbon atoms surrounding the point defect (vacancy). Vacancies can not, probably, be revealed in the positive contrast STM image as holes, because the contribution of the mechanical tip–sample interaction is higher than the contribution of the tunneling current to the measured corrugation and the effective number of atoms contributing to the corrugation is higher than one. This can be supported by the experiments performed to measure the corrugation amplitude as a function of the tunneling gap resistance and therefore the tip–sample separation.[23] It has been shown that at a small bias voltage (*i.e.* small tip–sample distance) the corrugation amplitude is dominated by the forces between tip and surface (mechanical tip–sample interaction). Using the contrast inversion, taking into account the "hollow-site imaging", it is possible to depict single atom defects as illustrated in Fig. 7(a). This may explain the vacancy-like feature seen in the inverted image depicted in Fig. 7(b) (marked by an arrow). Furthermore, the similarity is striking between the hexagons seen in the inverted STM image and those observed in the HRTEM micrograph (Fig. 2).

Conclusion

We have discussed a possible imaging mechanism of graphite based on mechanical considerations, in which tip–surface interactions, local surface elastic deformation, and local hardness were addressed. We showed that the observed corrugation is a result of convolution of $\rho(r, E_f)$ and local mechanical deformation of the surface.[23,59] The contribution of the local-induced deformation to the positive image contrast is higher than that of the local density of states ($\rho(r, E_f)$), leading to a pronounced appearance of the holes in the STM image, due to the variation in the local hardness between A-, B- and hole-

sites (a hole is harder than an A- and an A-site is harder than a B-site). The STM thus "sees" the hitherto neglected hollow sites in the graphite structure and not the atom positions. This imaging mechanism can also be used to understand the corrugations observed when strongly adsorbed C_{60} fullerene molecules were imaged by STM with intramolecular atomic resolution[60–62] as well as to clarify the reason for the appearance of only three atoms of the hexagonal-ring structure of the walls in nanotubes.[63–68] To visualize the true position of the carbon atoms in a hexagon we suggested inverting the measured STM image. We showed that atomic-size defects (*e.g.* point defects, vacancies) appear in the positive contrast STM images as protrusions. Vacancies can not be revealed in the positive contrast as holes, because the contribution of the mechanical tip–sample interaction to the measured corrugation is higher than that of the tunneling current. They can, however, be depicted in STM images with negative contrast. These structures also include, however, "information" from the close surrounding area (*i.e.* functional groups). Of course, the amount of the contribution to the "atomic" corrugation depends not only on the number of the surface carbon atoms involved in the mechanical tip–sample interaction but also on other parameters such as tip radius and shape, contaminants, and nature of tip–sample interactions, *etc.*

The present work shows how the controversial views on the striking anomaly of atomic resolution images of graphite can be resolved. We do not need to assume the presence of electronically inequivalent carbon atoms, for which there is no indication from any spectroscopic technique applied to date in probing the local electronic structure of sp^2 carbon atoms. Finally, it becomes apparent that the STM of graphite contains a significant contribution from mechanical effects and is not a method that responds to local electronic structure only.

References

1 A. Selloni, P. Carnevali, E. Tosatti and C. D. Chen, *Phys. Rev., B*, 1985, **31**, 2602.
2 G. Binnig, H. Fuchs, C. Gerber, H. Rohrer, E. Stoll and E. Tosatti, *Europhys. Lett.*, 1986, **1**, 31.
3 S.-I. Park and C. F. Quate, *Appl. Phys. Lett.*, 1986, **48**, 112.
4 G. Binnig, H. Rohrer, C. Gerber and E. Weibel, *Phys. Rev. Lett.*, 1982, **49**, 57.
5 H. J. Mamin, E. Ganz, D. W. Abraham, R. E. Thomson and J. Clarke, *Phys. Rev., B*, 1986, **34**, 9015.
6 R. Wiesendanger and D. Anselmetti, in *Scanning Tunneling Microscopy I*, ed. H.-J. Güntherodt and R. Wiesendanger, Springer, Berlin, 1992, vol. 1, p. 131.
7 H. A. Mizes, S.-I. Park and W. A. Harrison, *Phys. Rev., B*, 1987, **36**, 4491.
8 K. Kobayashi and M. Tsukada, *J. Vac. Sci. Technol., A*, 1990, **8**, 170.
9 F. Atamny and A. Baiker, *Appl. Catal. A*, 1998, **173**, 201.
10 D. Tomanek, S. G. Louie, H. J. Mamin, D. W. Abraham, R. E. Thompson, E. Ganz and J. Clarke, *Phys. Rev., B*, 1987, **35**, 7790.
11 D. Tomanek and S. G. Louie, *Phys. Rev., B*, 1988, **37**, 8327.
12 J. Tersoff, *Phys. Rev. Lett.*, 1986, **57**, 440.
13 A. L. Tchougreeff and R. Hoffmann, *J. Phys. Chem.*, 1992, **96**, 8993.
14 The site asymmetry A is defined, according to Tomanek *et al.* (*Phys. Rev. B*, 1987, **35**, 7790), as $A = [I(B) - I(A)]/[I(B) + I(A)]$: where $I(A)$ is the tunneling current at A sites and $I(B)$ at B sites. The tunneling current is expressed by Tersoff and Hamann (*Phys. Rev. Lett.*, 1983, **50**, 1998; *Phys. Rev. B*, 1985, **31**, 805) as $p \sim I$, where p is the local density of states.
15 J. Tersoff and D. R. Hamann, *Phys. Rev., B*, 1985, **31**, 805.
16 M.-H. Whangbo, W. Liang, J. Ren, S. N. Magonov and A. Wawkuschewski, *J. Phys. Chem.*, 1994, **98**, 7602.
17 K. H. Lee, M. Causa and S. S. Park, *J. Phys. Chem., B*, 1998, **102**, 6020.
18 T. A. Land, T. Michely, R. J. Behm, J. C. Hemminger and G. Consa, *Surf. Sci.*, 1992, **264**, 261.
19 S. P. Kelty and C. M. Lieber, *Phys. Rev., B*, 1989, **40**, 5856.
20 S. P. Kelty and C. M. Lieber, *J. Phys. Chem.*, 1989, **93**, 5983.
21 D. Anselmetti, V. Geiser, D. Brodbeck, G. Overney, R. Wiesendanger and H.-J. Güntherodt, *Synth. Met.*, 1990, **38**, 157.
22 M. Kuwabara, D. R. Clarke and D. A. Smith, *Appl. Phys. Lett.*, 1990, **56**, 2396.
23 J. M. Soler, A. M. Baro, N. Garcia and H. Rohrer, *Phys. Rev. Lett.*, 1986, **57**, 444.
24 C. M. Mate, R. Erlandsson, G. M. McClelland and S. Chiang, *Surf. Sci.*, 1989, **208**, 473.
25 M. Salmeron, D. F. Ogletree, C. Ocal, H. C. Wang, G. Neubauer, W. Kolbe and G. Meyers, *J. Vac. Sci. Technol., B*, 1991, **9**, 1347.
26 J. B. Pethica, *Phys. Rev. Lett.*, 1986, **57**, 3235.
27 I. P. Batra, N. Garcia, H. Rohrer, H. Salemink, E. Stoll and S. Ciraci, *Surf. Sci.*, 1987, **181**, 126.
28 D. P. E. Smith, G. Binnig and C. F. Quate, *Appl. Phys. Lett.*, 1986, **49**, 1166.
29 R. Schlögl, in *Handbook of Heterogeneous Catalysis*, ed. G. Ertl, H. Knözinger and J. Weitkamp, VCH, Weinheim, 1997, vol. 1, p. 138.
30 U. Müller, *Inorganic Structural Chemistry*, Wiley, New York, 1993.
31 S. A. Gould, K. Burke and P. K. Hansma, *Phys. Rev., B*, 1989, **40**, 5363.
32 I. P. Batra and S. Ciraci, *J. Vac. Sci. Technol., A*, 1988, **6**, 313.
33 F. Abraham and I. P. Batra, *Surf. Sci.*, 1989, **209**, L125.
34 T. R. Albrecht and C. F. Quate, *J. Appl. Phys.*, 1987, **62**, 2599.
35 T. R. Albrecht, M. M. Dovek, M. D. Kirk, C. A. Lang, C. F. Quate and D. P. E. Smith, *Appl. Phys. Lett.*, 1989, **55**, 1727.
36 B. Parkinson, *J. Am. Chem. Soc.*, 1990, **112**, 7498.
37 E. Delawski and B. A. Parkinson, *J. Am. Chem. Soc.*, 1992, **114**, 1661.
38 O. M. Leung and M. C. Goh, *Science*, 1992, **255**, 64.
39 H. Hiura, T. W. Ebbesen, J. Fujita, K. Tanigaki and T. Takada, *Nature*, 1994, **367**, 148.
40 T. W. Ebbesen and H. Hiura, *Adv. Mater.*, 1995, **7**, 582.
41 H. V. Roy, C. Kallinger and K. Sattler, *Surf. Sci.*, 1998, **407**, 1.
42 H.-V. Roy, C. Kallinger, B. Marsen and K. Sattler, *J. Appl. Phys.*, 1998, **83**, 4695.
43 T. M. Bernhardt, B. Kaiser and K. Rademann, *Surf. Sci.*, 1998, **408**, 86.
44 G. Binnig, *Specul. Sci. Technol.*, 1987, **10**, 345.
45 Z. Y. Rong, *Phys. Rev., B*, 1994, **50**, 1839.
46 A. Tracz, A. A. Kalachev, G. Wegner and J. P. Rabe, *Langmuir*, 1995, **11**, 2840.
47 G. Bräuchle, S. Richard-Schneider, D. Illig, J. Rockenberger, R. D. Beck and M. M. Kappes, *Appl. Phys. Lett.*, 1995, **67**, 52.
48 R. T. Yang, in *Chemistry and Physics of Carbon*, ed. P. A. Thrower, Marcel Dekker, New York, 1984, vol. 19, p. 163.
49 H. Chang and A. J. Bard, *J. Am. Chem. Soc.*, 1990, **112**, 4598.
50 H. Chang and A. J. Bard, *J. Am. Chem. Soc.*, 1991, **113**, 5588.
51 B. Henschke, H. Schubert, J. Blöcker, F. Atamny and R. Schlögl, *Thermochim. Acta*, 1994, **234**, 53.
52 M. R. Soto, *J. Microsc.*, 1988, **152**, 779.
53 H. A. Mizes and W. A. Harrison, *J. Vac. Sci. Technol., A*, 1988, **6**, 300.
54 M. R. Soto, *Surf. Sci.*, 1990, **225**, 190.
55 H. A. Mizes and J. S. Foster, *Science*, 1989, **244**, 559.
56 N. Takeuchi, J. Valenzuela-Benavides and L. M. d. l. Garza, *Surf. Sci.*, 1997, **380**, 190.
57 J. Valenzuela-Benavides and L. M. d. l. Garza, *Surf. Sci.*, 1995, **330**, 227.
58 F. Ohnesorge and G. Binnig, *Science*, 1993, **260**, 1451.
59 J. H. Coombs and J. B. Pethica, *IBM J. Res. Dev.*, 1986, **30**, 455.
60 H. P. Lang, V. Thommen-Geiser, C. Bolm, M. Felder, J. Frommer, R. Wiesendanger, H. Werner, R. Schlögl, A. Zahab, P. Bernier, G. Gerth, D. Anselmetti and H.-J. Güntherodt, *Appl. Phys., A*, 1993, **56**, 197.
61 S. Behler, H. P. Lang, S. H. Pan, V. Thommen-Geiser and H.-J. Güntherodt, *Z. Phys., B*, 1993, **91**, 1.
62 X. Yao, T. G. Ruskell, R. K. Workman, D. Sarid and D. Chen, *Surf. Sci.*, 1996, **367**, L85.
63 M. Ge and K. Sattler, *Science*, 1993, **260**, 515.
64 J. W. G. Wildöer, L. C. Venema, A. G. Rinzler, R. E. Smalley and C. Dekker, *Nature*, 1998, **391**, 59.
65 T. A. Odom, J.-L. Huang, P. Kim and C. M. Lieber, *Nature*, 1998, **391**, 62.
66 H. Beyer, M. Müller and T. Schimmel, *Appl. Phys., A*, 1999, **68**, 163.
67 L. C. Venema, J. W. G. Wildöer, J. W. Janssen, S. J. Tans, H. L. J. T. Tuistra, L. P. Kouwenhoven and C. Dekker, *Science*, 1999, **283**, 52.
68 L. C. Venema, J. W. G. Wildöer, C. Dekker, G. A. Rinzler and R. E. Smalley, *Appl. Phys., A*, 1998, **66**, 153.

Paper 9/04657G